

Received May 31, 2017, accepted June 23, 2017, date of publication August 11, 2017, date of current version March 15, 2018.

Digital Object Identifier 10.1109/ACCESS.2017.2724304

Environmental Model-Based Time-Reversal Underwater Communications

LUSSAC P. MAIA, ANTÓNIO SILVA, AND SÉRGIO M. JESUS, (Member, IEEE)

Laboratory of Robotic Systems in Engineering and Science, Campus de Gambelas, Universidade do Algarve, 8005-139 Faro, Portugal

Corresponding author: Lussac P. Maia (lussacmaia@gmail.com)

This work was supported in part by the Foreign Courses Program of Brazilian Navy under Grant PCEExt-Port219/EMA and in part by the EU H2020 Research Program through the STRONGMAR Project under Contract 692427.

ABSTRACT This paper addresses channel compensation in underwater acoustic communications by proposing a method for inserting physical propagation modeling into a passive time-reversal (PTR) receiver. PTR is known as a low complexity channel equalizer that uses multichannel probing for time signal refocusing, reducing inter-symbol interference caused by multipath propagation. The proposed method aims to improve PTR communications performance by replacing the conventional noisy channel estimates with optimized and noiseless channel replicas computed by a numerical ray trace model. The optimization consists of environmental focalization in an “*a priori*” physical parameter search space to obtain “*a posteriori*” channel impulse response replicas that best match the observed data. The results obtained on two data sets acquired during the UAN’11 experiment in a shallow water fjord near Trondheim, in May 2011, show that the proposed method clearly outperformed the traditional PTR by a mean square error gain from 1 up to 4 dB. Channel tracking was effective despite a reduced physical parameter search space that could be exhaustively covered with a minimal computational effort. To the best of our knowledge, this is the first successful report on the usage of a physical parameter fed numerical model for underwater acoustic communications channel equalization with real transmitted data in a useful underwater modem frequency band.

INDEX TERMS Underwater acoustic communications, time-reversal, channel estimation, environmental focalization, coherent equalization.

I. INTRODUCTION

The last two decades have seen significant advances in autonomous underwater sensing platforms, widening their capabilities for complex long range missions. A crucial aspect for this success is their ability to reliably communicate over a rapidly changing underwater acoustic channel. The update rate and complexity of channel equalization has been and still is a central issue in underwater communications.

Equalization of underwater communication channels at high data rate is challenging, and particularly difficult in the shallow water case, characterized by a double time-delay and frequency spread. Channel distortion is often attributed to one or more of the following effects: multipath propagation, time compression/dilation induced by relative source-receiver motion and wind-driven acoustic scattering at the sea surface.

A well-known and widely used technique for channel equalization is the Decision Feedback Equalizer (DFE) [1]. The DFE fits the channel with a nonlinear adaptive filter which coefficients are estimated to compensate for channel distortions, following an iterative procedure often used in

aerial wireless communications [2]. However, unlike in aerial channels, in multipath prone underwater channels, convergence problems inherent to the iterative algorithm may occur in adaptive equalization, especially when using long frames [3]. The DFE can also be implemented in multi-channel receivers, as proposed in in [4] and [5]. A rather different technique is the Passive Time Reversal (PTR) [6], which is a low complexity receiver that uses multichannel probing for time signal refocusing, effectively reducing inter-symbol interference (ISI) caused by multipath propagation. PTR assumes that a receiving array is available and that it captures a significant portion of the energy propagating in the water column [7]–[10]. In its conventional form, PTR is based in data derived channel impulse response (CIR) estimates and its performance is limited by noise (in the CIR estimates) and by channel variability. Since PTR has limited focusing capability [11], it is common to supplement it with single channel linear equalization. Although adaptive PTR techniques were developed [12], [13], it is still seen more as a channel pre-processor than as a full channel equalizer.

The motivation of this work is to improve PTR as a full channel equalizer by increasing its performance through a link with the physics of acoustic propagation. The current coherent form to include physical parameters in underwater acoustics is via numerical propagation models. Although, numerical models have been rarely used in underwater acoustic communications, they have been proven successful in, nowadays popular, techniques such as matched-field processing (MFP) for source localization, initially proposed by [14] and [15], (see details in [16] and an overview in [17] and references therein), ocean acoustic tomography (OAT) [18], [19] and matched-field inversion (MFI) for generic environmental parameter estimation [20], [21]. There exists a large body of work (impossible to fully cite here), with a variety of processing techniques with their particularities and application fields, but they all have one common feature: they feed environmental information in numerical models and compare the output to experimental data. In that sense these techniques are often called as “model-based” as opposed to “data-driven” only. Many studies carried out with model-based techniques refer the difficulties to favorable compare modeled and experimental data in the high frequency range, say, above 2 kHz. This seems to be the reason why, to the best of the authors knowledge, there are no reports on the usage of numerical models to design CIR replicas for channel equalization in underwater acoustic communications with real data.

This work proposes a communication channel PTR equalization method based on physical modeling, hereby named as Environmental-based Passive Time Reversal (EPTR). The approach inserts a high-frequency acoustic propagation model in the process of obtaining CIR replicas that best match the observed data for time-reverse filtering. This is performed through an environmental focalization algorithm running on an “a priori” physical parameter space to obtain the “a posteriori” best candidate CIR replicas. Thus, noisy channel estimates are substituted by the best fit noiseless channel replicas computed by the physical model.

Results obtained with EPTR and conventional pulse-compressed PTR (PC-PTR) on real data records acquired in two days of May 2011 during the UAN’11 experiment in Trondheim (Norway), show that EPTR clearly outperformed the conventional PC-PTR by an amount of 1 to 4 dB in mean-square error (MSE). More important than the actual comparative performance, that may vary from case to case, these results show that environmental model-based methods may be used with success on real data underwater communications, are robust and may efficiently use *a priori* environmental information and therefore potentially track a changing environment.

This paper is organized as follows: Section II describes the model-based methodology driven by environmental focalization. Section III describes the UAN’11 experiment and discusses the experimental results with coherent communications processed by PC-PTR and EPTR. Section IV concludes the paper.

II. MODEL-BASED PASSIVE TIME REVERSAL WITH ENVIRONMENTAL FOCALIZATION

In this section the conventional PC-PTR receiver is modified to include an environmental focalization algorithm that employs a forward ray tracing model which input parameters are adjusted to best match the channel CIR. The Bellhop and Bounce models [22] are jointly employed to simulate acoustic propagation of communication signals in a range dependent ocean wave-guide with layered seabed, where the former computes amplitudes and delays of arrival paths and the latter computes reflection coefficients of the layered bottom. In the next sub-sections the assumed data model and the plain PC-PTR algorithm is introduced first and then the environmental focalization processor is described in detail.

A. DATA MODEL FOR PASSIVE TIME REVERSAL IN COHERENT UNDERWATER COMMUNICATIONS

A bit stream message $m[l]$ is digitally modulated with a phase shift key scheme, up-sampled and filtered with a pulse shape low pass filter $p[n]$, so that after heterodyne to the carrier frequency F_c the pass-band signal generated for transmission is

$$\tilde{s}(t) = \sum_n \text{Re} \left[s(t - nT_b) e^{j2\pi F_c t} \right], \quad (1)$$

where the base-band signal is

$$s[n] = \sum_l a[l] p[n - lT_s], \quad (2)$$

and the MPSK message is

$$a[l] = e^{j2\pi(m[l]-1)/M}, \quad m[l] \in [1, \dots, M] \quad (3)$$

with the base-band sampling interval being denoted as T_b , the symbol interval as T_s , M as the symbol map size and Re denotes real part.

The time-variant CIR for a particular source-receiver transect can be represented by the two-dimensional complex base-band variable $h[n, k]$, where the discrete delay-dimension k is the reduced time CIR snapshot coordinate, while several sequential snapshots may be recovered along the discrete true time variable n . Note that each CIR snapshot represents a state of the time-variant channel in a particular time instant and its replica can be modeled by computing the path gain and delay pair generated by an appropriate underwater acoustic propagation model. In the case of a linear time-invariant system the received signal is calculated by the convolution between the impulse response and the transmitted signal, but in a time-variant system this is not valid. Instead, an integral operation that performs time-variant filtering must be done. Thus, assuming hereafter a complex base-band equivalent representation, the noisy received signal $y[n]$ is given by

$$y[n] = \sum h[n, k] s[n - k] + w[n], \quad (4)$$

where $w[n]$ denotes additive random noise. Using matrix notation, (4) can be rewritten as a function of CIR snapshots.

Assuming that $\mathbf{s} \in \mathbb{C}^{K \times 1}$, $\mathbf{H} \in \mathbb{C}^{P \times J}$, $\mathbf{g} \in \mathbb{C}^{J \times 1}$ one can form $\mathbf{H}^T = [\mathbf{g}_1, \mathbf{g}_2, \dots, \mathbf{g}_P]$, where \mathbf{g}_p is the p -th snapshot and $P = K + J - 1$. Thus, the discrete time-variant system is

$$\mathbf{y} = \text{diag}(\mathbf{S}\mathbf{H}^T) + \mathbf{w}, \quad (5)$$

where matrix \mathbf{S} has a Toeplitz structure being computed from zero-padded \mathbf{s} with $\mathbf{S} \in \mathbb{C}^{P \times J}$.

Moreover, note that when the Doppler effect *e.g.* due to sensor motion is sufficiently compensated for, then the snapshots are kept invariant along time and the received signal becomes

$$y[n] = \sum_k g[k]s[n-k] + w[n] = s[n] * g[k] + w[n], \quad (6)$$

where $g[k] \simeq h[0, k]$ if assumed as an initial snapshot, or still $g[k] \simeq \bar{h}[n, k]$ if assumed as an average snapshot (which is the case in this work), and where symbol $*$ denotes convolution.

Since the PC-PTR equalizer performs time-reversal matched-filtering of the received signals on each channel using the CIR estimates, its output is the sum

$$z[n] = \sum_l z_l[n] = \sum_k Q[n]I[n-k] \quad (7)$$

with

$$I[n] = \sum_k s[k]R[n-k]; \quad R[n] = \sum_k p^*[k]p[n-k] \quad (8)$$

and

$$Q[n] = \sum_l \sum_k \hat{g}_l^*[k]g_l[n-k] \quad (9)$$

The R -function is the auto-correlation of the pulse shape and the I -function is defined by the convolution of the R -function and the transmitted signal. The Q -function represents the cross-correlation between the estimated and the actual CIR. The Q -function is particularly useful as an indicator of the PC-PTR performance, since an impulse-like shape generally means a successful compensation of the multipath distortion. The present work processes real data which precludes to know the actual CIR, however an equivalent criterion is used for measuring the PC-PTR performance by computing its output average power.

1) BACKGROUND IN STANDARD PASSIVE TIME REVERSAL

Aiming to make it more clear the above presented standard time-reversal model to readers not familiar with it, the next three paragraphs shortly discusses a basic background in time-reversal acoustics applied to time-reversal underwater communications.

Two essential properties of acoustic waves are that (i) when two waves pass through the same location, they have constructive interference (reinforce each other) if their peaks and troughs correspond, and they have destructive interference (tend to cancel each other out) if the peaks of one combine with the troughs of the other; and (ii) the underlying

physical processes of waves would be unchanged if time were reversed (reciprocity principle of the wave equation). The former property often occurs in shallow water multipath propagation, where echoes reflect back from boundaries, mixing together different portions of the same wave so that a single transmitted pulse generates multiple copies of itself at the receiver. The latter property, that makes the time-reversed acoustics method possible, can be observed by employing an active Time-Reversal Mirror (TRM) composed by a vertical line of transducers spanning in the water column to capture the main modes of propagation. A signal transmitted by a source is captured by the TRM transducers and then the reverse version of the received signals are retransmitted causing the energy refocuses to the same position of the source, no matter the complexity of the channel.

The passive time-reversal method, described in [8] and in a large body of work in the literature, relies on mode orthogonality (just as the active TRM), but instead of reverse signal retransmission, it uses channel estimates to synthetically perform a virtual ocean response match through the use of conjugate reverse filtering and mixing. Despite its simplicity, it requires a sufficiently long and dense array to reduce ISI, avoiding poor sampling of the high-order modes and subsequent orthogonality property violation. The CIR estimates are typically obtained by correlating each received distorted probe signal with the transmitted probe signal, resulting in a noisy estimate of the channel Green's function. Such standard CIR estimation technique is equivalent to the pulse compression (PC), commonly used by radar and sonar to increase the range resolution and the signal to noise ratio.

Therefore, the standard PC-PTR receiver in the presence of a noisy environment involves the filtering of stochastic received signals by deterministic or stochastic CIR, whose accuracy directly affects the performance of the time-reversal method to reduce ISI.

B. THE ACOUSTIC FOCALIZATION PROCESSOR

The EPTR is based on an acoustic focalization processor that aims at generating noise free channel replicas for time-reversal matched-filtering implementation of the PC-PTR. This focalization is done over a given number of environment candidates and selects those that best match the pulse-compressed CIR estimate extracted from the observed data. In order to clarify this, Fig. 1 shows the complete block diagram of a single-input-multiple-output coherent communication receiver based on the EPTR processor. The standard passive time-reversal is obtained with the switch in PC-PTR mode, where the pulse-compressed (PC) CIR estimates are directly used for matched-filtering each Doppler compensated array channel and the outputs are coherently summed. In EPTR mode, the PC estimated CIRs are used to select the "a posteriori" replicas from within an ensemble of possible channel responses generated from an "a priori" search space defined through a set of environmental parameters. This process of tweaking the environmental parameters to obtain a noise-free numerical model generated channel response that

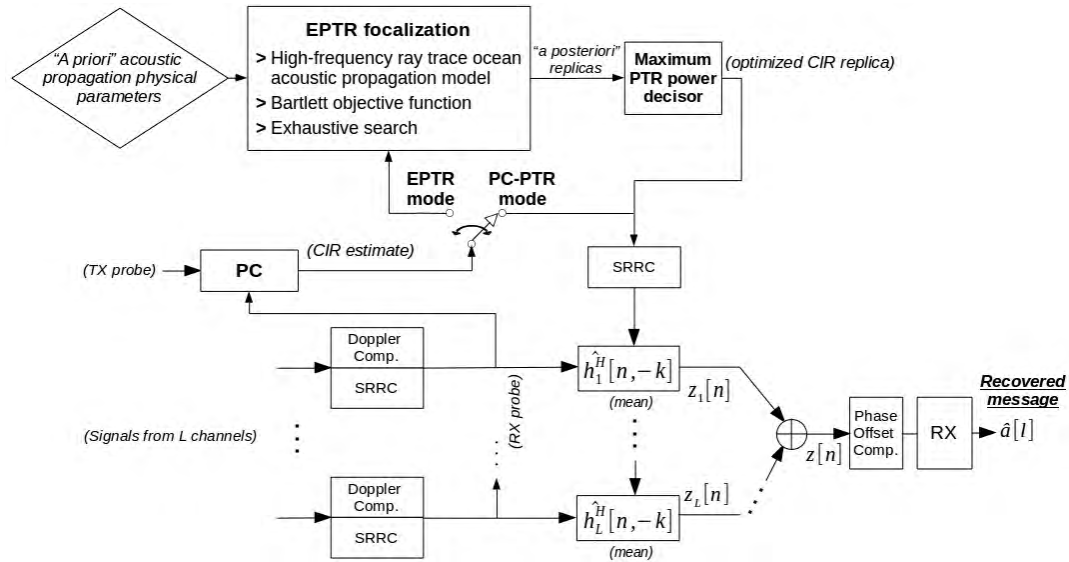


FIGURE 1. Block diagram of a single-input-multiple-output coherent communication receiver allowing for the implementation of either the standard pulse compressed Passive Time-Reversal or the Environmental-based Passive Time Reversal processors (see text for detailed explanation of the role of each block). SRRC is the square root raised cosine pulse shape filter.

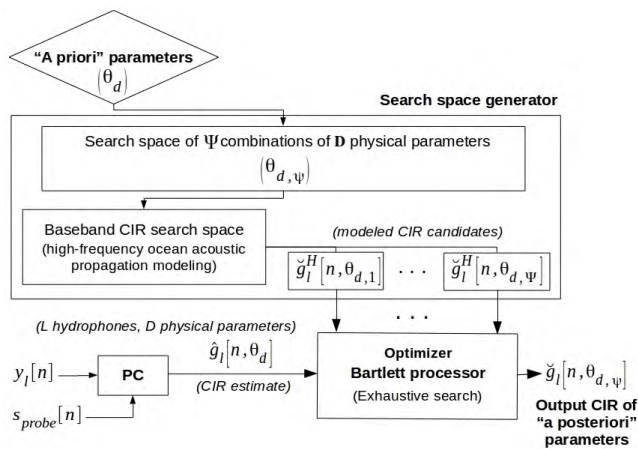


FIGURE 2. Block diagram of the environmental focalizer for EPTR implementation.

best matches the observed channel, is termed “environmental focalization”. The detail of the environmental focalizer block section is given in the diagram of Fig. 2. The “a priori” physical parameters are provided by the user to the focalization block, in which the core optimization is performed. In general, it is important to note that environmental focalization results depend on an appropriate choice of “a priori” search space data. For instance, the use of a search space too large can generate ambiguity and an unrealistic set of “a posteriori” CIRs, making the channel compensation to fail due to modeling errors. Successful results depend, in some degree, on an appropriate choice of the search space from a physical viewpoint, which can be complemented by prior environmental assessment of the area of interest with

dedicated equipment. These parameters should be chosen based on in-situ measurements or background historical data. The choice of the set of environmental parameters to be included in the search space is a compromise between a meaningful CIR model to mimic channel variability and the computational load to run the optimization. A high number of optimization parameters may become quickly computationally prohibitive. These two objectives converge to selecting environmental parameters along a well known hierarchical list from the most to the least influential parameters on the output modeled acoustic field. This hierarchy is known to put on top of the list the geometrical parameters as for example source depth, source-receiver range, and receiver depth. On top of the most influential environment-related parameters are the water column sound speed and the compressional speed on the upper sediment layer. Then, parameter selection becomes very case dependent and there is no generic rules so, this is often based on a trial and error for fine tuning of the focalization procedure. The basic rule is that the search space should be just wide enough to capture the channel variability during the transmission time frame. Another time frame, another day, or *a fortiori*, another location would, in principle, require readjustment of the parameter search space. More on this in section III.

The optimization was performed using a Bartlett objective function to select a small refined set of CIR candidates that best correlate with the pulse-compressed estimated observed CIR. The objective function employed in this work is defined in time-domain by

$$B(\psi) = \frac{\check{g}_l^H[n, \theta_{d,\psi}] C[n, \theta_d] \check{g}_{l,p}[n, \theta_{d,\psi}]}{\|g_l(n, \theta_d)\| \|\check{g}_l(n, \theta_{d,\psi})\|}, \quad (10)$$

with the covariance matrix of observed data being

$$C[n, \theta_m] = \frac{1}{P} \sum_{p=1}^P g_{l,p}[n, \theta_d] g_{l,p}^H[n, \theta_d], \quad (11)$$

where \check{g} denotes the predicted CIR data, g denotes observed CIR data, P is the number of observations, L is the number of hydrophones, θ_d is the d -th physical parameter and Ψ is the set of CIR replica candidates generated by the search space. Using the maximum a posteriori criterion, the best fitness candidate is computed by performing $B_{MAP} = \max_{\psi \in \Psi} B(\psi)$.

Furthermore, a Maximum Power Decisor is employed to test the CIR candidates “a posteriori” and select the CIR that maximizes the PTR output power. The maximum power parameters set ψ_{mp} is given by

$$\psi_{mp} = \arg \max_{\psi_{output}} \frac{1}{N} \sum_{n=0}^{N-1} \left| \sum_l \check{g}_l[n, \theta_d, \psi_{output}] * y_l^\dagger[-n] \right|^2 \quad (12)$$

where $*$ denotes convolution, \dagger denotes conjugate and ψ_{output} denotes the few set of parameters obtained as output of the inversion. Thus, the EPTR output signal is

$$z_{mp}[n] = \sum_l \check{g}_l[n, \theta_d, \psi_{mp}] * y_l^\dagger[-n] \quad (13)$$

Additionally to the focalization, and since time-reversal is limited to coarse ISI mitigation [11], post-processing in single channel is performed to compensate phase rotation, using probe-based mean phase estimation and complex conjugate compensation to the corresponding slot, as well as using least mean squares to minimize symbol recovery residual error.

III. EXPERIMENTAL DATA PROCESSING

A. THE UAN'11 EXPERIMENT

The Underwater Acoustic Network 2011 (UAN'11) experiment took place in Strindfjorden, Trondheim (Norway) during May 2011. See objectives and details of the experiment in [23]. During this experiment a network composed of several nodes, including both mobile (AUV mounted) and fixed (moored) transmitters/receivers, was deployed and operated during the whole period. Every node of the network was equipped with modified Kongsberg cNODE Mini modems and one of the nodes included a receiving only vertical array with 16 channels - the Sub-surface Telemetry Unit (STU). Detailed characteristics of the environment and the signals processed in this work are presented in the following subsections.

1) BATHYMETRY AND SOURCE / RECEIVER-ARRAY GEOMETRY

Fig. 3 shows the network nodes' positions superimposed on the bathymetry of the experiment test site. Various fixed nodes (FNO), the STU, the pier and two mobile nodes (OBJ) are shown. In the present work the data obtained on the

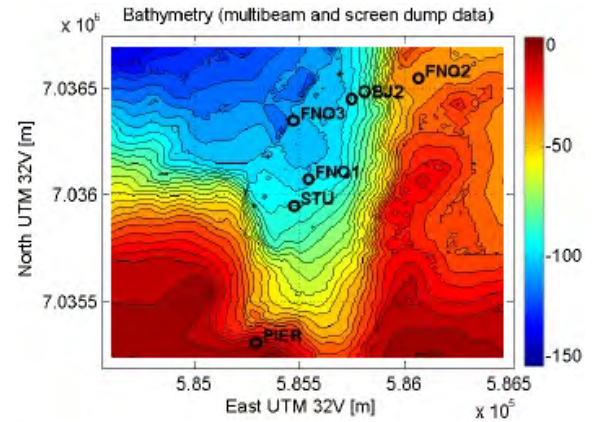


FIGURE 3. UAN'11 network node position superimposed on the bathymetry map of the area: FNO# denotes fixed nodes, STU is the Sub-surface Telemetry Unit multichannel array and OBJ# denote AUV mounted mobile nodes. The transect between FNO2 and the STU is 890 m long, and is range-dependent attaining a maximum depth of 100 meters.

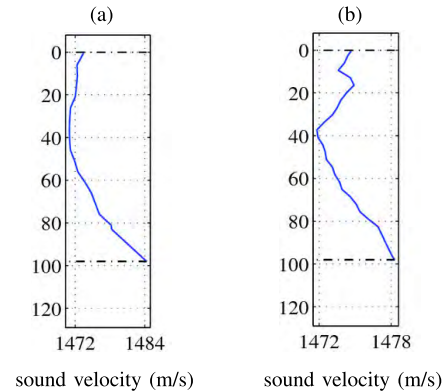


FIGURE 4. Sound velocity profiles measured with CTD#4 near the STU location on May 24 (a) and on May 27 (b), 2011.

transect between source node FNO2 and the receiving multi-channel array STU were analyzed. The source is at 28 m depth and 890 m away from a vertical line array of 16 hydrophones, 4 m equally spaced, spanning from 14.1 m to 74.1 m depth. Both the source and the receiving array are moored at the marked positions, therefore sensor movement is expected to be reduced to a small horizontal oscillation. In addition, the tide variation at the experiment site is less than 2 m, considered small relative to the water depth at the source of about 38 m and 98 m at the position of the receiving array.

2) SOUND SPEED PROFILES FOR DAYS MAY 24 AND MAY 27, 2011

Several Conductivity Temperature Depth (CTD) casts were made during the UAN11 sea test. The measurements made on May 24 and May 27 with CTD#4 located near the STU are used in this work. The two Sound Speed Profiles (SSP), are shown in Fig. 4. The figure shows upward refracting profiles with a initial formation of a mixed layer in the upper 40 m on May 27, that was not present on May 24. The mixing layer

TABLE 1. Environmental physical parameters for propagation modeling and focalization.

Physical parameter	Unit	Reference	Search	Size
Source-receiver range	(m)	890	870 - 910	5
Source depth	(m)	28.1	26.50 - 29.50	5
Array depth	(m)	14.1	13.10 - 15.10	5
Sound speed profile	(m/s)		(see Fig. 4)	
Sediment				
Thickness	(m)	5	-	-
Comp. speed c_{p1}	(m/s)	1550	1480 - 1620	10
Comp. attenuation α_{p1}	(dB/ λ)	0.8	0.60 - 1.00	2
Density ρ_1	(g/cm ³)	1.8	1.30 - 2.30	2
Bottom				
Comp. speed c_{p2}	(m/s)	2100	-	-
Shear speed c_{s2}	(m/s)	250	-	-
Comp. attenuation α_{p2}	(dB/ λ)	0.1	-	-
Shear attenuation α_{s2}	(dB/ λ)	2.5	-	-
Density ρ_2	(g/cm ³)	2	-	-

on May 27 probably occurred because of changes in weather conditions and due to the influence of fresh water from rivers flowing in the region near the fjord.

3) TRANSECT SCENARIO AND SEABED GEOACOUSTIC PROPERTIES

The FNO2 - STU 890 m transect is strongly range-dependent with water depth varying between 38 and 98 m. The bottom parameters were derived from historical information of the area of a “rock bottom covered by mud or clay” using the Hamilton relations and also compiling the information used in [23]. The adopted environmental model is composed of a 5 m thick sediment layer over a bottom half space, which characteristic parameters are listed in column “Reference” of Table 1. This table also shows in the last two columns, the search interval and number of discretization intervals, respectively, for those parameters included in the environmental focalization procedure discussed below.

In order to obtain a glimpse of the possible propagation conditions for an acoustic transmission between FNO2 and the STU, Fig. 5 shows the Bellhop/Bounce model computed eigenrays between the source location and each of the vertical array receivers along the transect with the following path color coding: direct (magenta), surface reflected (blue), seabed reflected (red) and surface-bottom reflected (gray). One can see that there are very few bottom-reflected rays (in red) reaching the hydrophones 6 to 9, in comparison to the surface-reflected rays (blue) that reach all hydrophones. This occurs due to a low slope bottom near the source followed by a high slope bottom, creating a shadow zone for bottom-reflected rays. For this reason, it is expected that the CIR will have a second arrival path with a higher frequency spread (due to free surface motion) than the first arrival path.

4) DATA FRAME STRUCTURE AND MODEM FEATURES

The transmissions at the FNO2 node were performed by a cNODE-Mini modem transponder model 34180 provided by Kongsberg Maritime (KM, Kongsberg, Norway) and

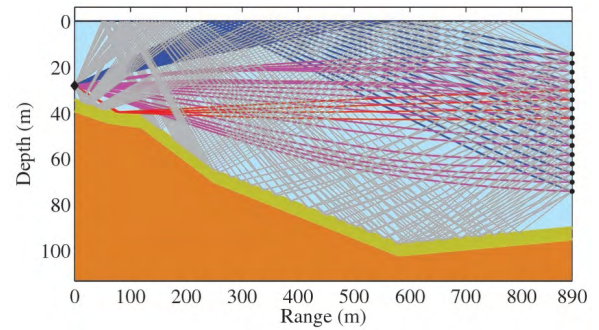


FIGURE 5. Scenario for the transmitter-receivers transect (FNO2-STU): range-dependent 890 m long transect, source depth 28.1 m, 16 hydrophones vertical array 4 m equally spaced from 14.1 m to 74.1 m depth, maximum water depth 100 m, 5 m sediment layer (in dark-yellow color) over bottom half-space (in orange color). The eigenrays are color coded as follows: direct paths in magenta, surface-reflected paths in blue, bottom-reflected paths in red, and surface-bottom-reflected paths in gray.

TABLE 2. Frame structure of the transmitted data stream.

Type	Preamble	Header	M-seq. + Message slot	Postamble
Size	511	40	(20 times)	511

specifically adapted to tasks of the UAN’11 experiment [23]. This acoustic modem is described in detail in [24] and it has a 180 beam pattern transducer at a center frequency of 25.6 kHz, with a bandwidth of 8 kHz and an emitted power between 173 and 190 dB re 1 μ Pa@1m.

During days May 24 and 27, the message data were the pixels of a gray image, converted into a bit stream QPSK modulated at a data rate of 4000 bps. The data frame structure is shown in Table 2 and has a total size of 50000 symbols, thus containing 100000 bits. The structure of this data frame is organized (in order) as a preamble m-sequence with 511 symbols, an header with 40 symbols, a payload and postamble m-sequence with 511 symbols. The preamble and postamble are used to perform time compression/dilation compensation, aiming at removing clock synchronization impairments between transmitter and receiver and a possible Doppler trend. The payload contains the bit-stream message corresponding to the image pixels and a sequence of 20 short m-sequences with 127 symbols each, which are inserted every 1 second for channel tracking. In addition to channel tracking, these short m-sequences are used for PC-PTR and EPTR CIR estimation through PC and environmental focalization, respectively. The final channel matched-filtering in the time-reversal receiver is performed with the mean CIR over the 20 short m-sequence estimate, both for PC-PTR and EPTR. Further, since the bit stream length is variable according to a particular message or set of image pixels and the frame size is fixed (50000 symbols), a constant stream of the symbol 1 is positioned at the end of the payload with the length needed to complete the frame size. Fig. 6 shows the spectrogram of a signal received at the deepest hydrophone where the constant stream is seen as a tone at the carrier frequency after the

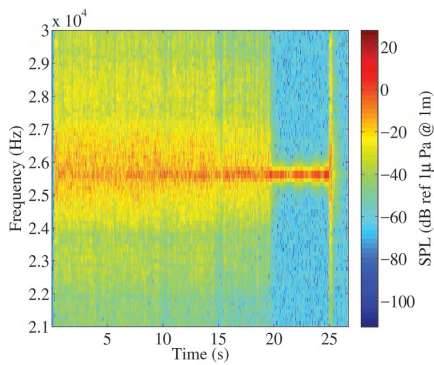


FIGURE 6. Spectrogram of a signal received at hydrophone 1 (deepest), with sound pressure level (SPL) in decibel referred to $1\mu Pa$ at 1 m. Carrier frequency 25.6 kHz. The constant stream of 1's is filling the data packet between 20 and 25 seconds.

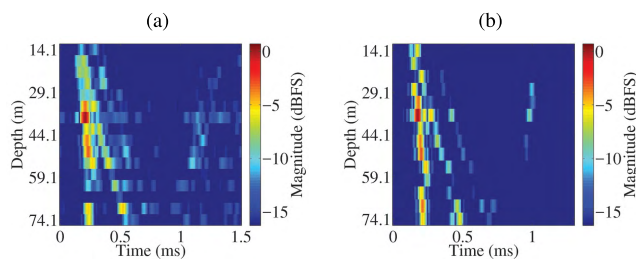


FIGURE 7. Wavefront estimated by PC-PTR (a) and by EPTR focalization (b) for May 24 data. The colorbar shows magnitude in decibel referred to full scale (dBFS).

payload end and before the final postamble, between 20 and 25 seconds.

B. EPTR EXPERIMENTAL RESULTS AND DISCUSSION

This section presents the results of PC-PTR and EPTR in the experimental data acquired during the UAN’11 experiment in days May 24 and 27, 2011.

1) ANALYSIS OF TIME-VARIANT CIR DATA

The first point to be verified is the time-variant CIR, obtained by PC of the received signals using the transmitted probes, after polyphase resampling (Doppler compensation block in Fig. 1). Fig. 7 shows the wavefronts estimated with PC (a) and modeled after environmental focalization (b) for data of May 24, in a 16 ms time window. The wavefronts show that two arrivals are clearly distinguished with a relatively good match between data and model. The water wavefront has a clear maximum of energy at the minimum of the sound speed while the second wavefront is downward propagating. Clearly the wavefronts estimated with PC-PTR show noise while those obtained with EPTR are noiseless and therefore much better defined.

Fig. 8 shows, for the data collected on May 24 at the hydrophone 6 (54.1 m depth), the CIR estimated with PC in time-delay representation along the 20 seconds (a), the mean CIR estimated power (b), the CIR modeled by EPTR using environmental focalization in time-delay representation (c)

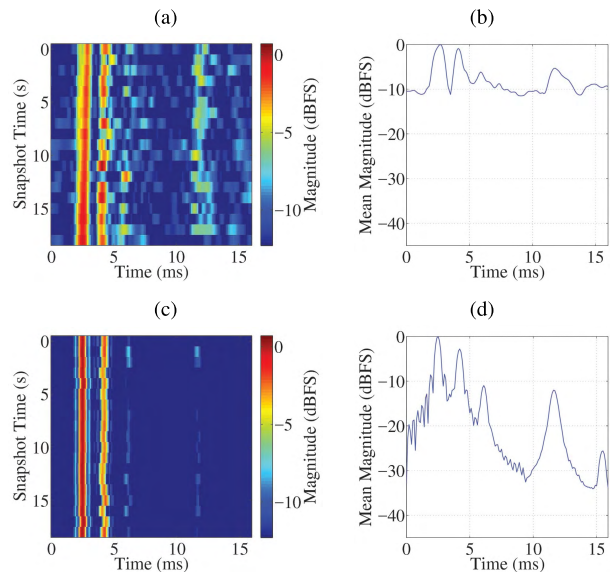


FIGURE 8. CIR for the data collected on May 24 at hydrophone 6 (54.1 m depth) estimated by pulse compression (a) and (b) and modeled through environmental focalization with EPTR (c) and (d). Time-delay CIR representation (a) and (c) and average magnitude CIR (b) and (d). The colorbar shows normalized magnitude in dBFS.

and the mean CIR modeled power by EPTR (d). Comparing plots 8 (a) and (c), a good match is clearly visible between path arrival times and amplitudes. There is a considerable amount of noise on the observed data, which tends to obscure the secondary paths with smaller magnitude. As expected, comparing the first and second rows in Fig. 8, the noise reduction is clearly noted.

Fig. 9 shows the same type of plots as Fig. 8 but for the data set of May 27. Again in this case and despite the very different sound velocity profiles (Fig. 4), the capture of the overall path arrival structure as well as the small scale variability is striking in the modeled data of Fig. 9, plots (c) and (d), when compared to plots (a) and (b), respectively. Note, however, a small discrepancy on the mean arrival time of the late path at around 14 ms delay when comparing plots (b) and (d). Fig. 10 compares the baseband complex envelope estimated with PC with that obtained by EPTR focalization for snapshot 4 of May 27, hydrophone 6. This comparison illustrates the much lower noise level on the “a posteriori” modeled CIR snapshot, when compared to the corresponding pulse-compressed estimate.

2) “A POSTERIORI” PHYSICAL PARAMETERS

A second point to be checked is the set of physical parameters resulting from acoustic modeling optimization. The physical parameters that best match the observed data are obtained as output of the acoustic focalization algorithm after an exhaustive search over the parameter space defined in columns “Search” and “Size” of table 1. The dimension of the search space is 5000. Although the focus of this work is not on environmental inversion, the obtained “a posteriori” physical

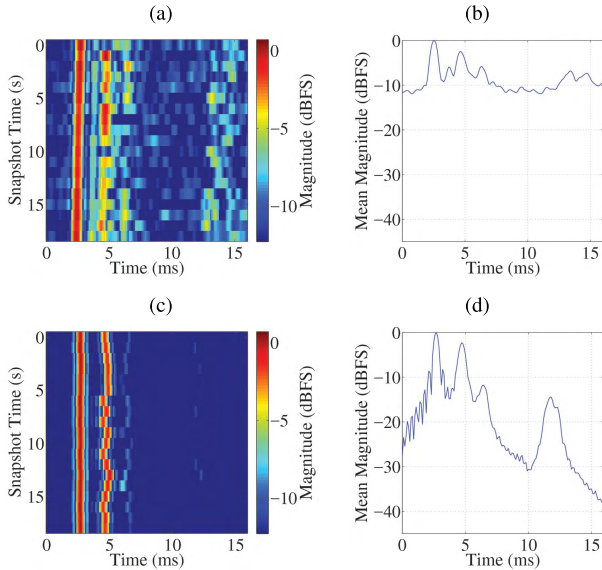


FIGURE 9. CIR for the data collected on May 27 at hydrophone 6 (54.1 m depth) estimated by pulse compression (a) and (b) and modeled through environmental focalization with EPTR (c) and (d). Time-delay CIR representation (a) and (c) and average magnitude CIR (b) and (d). The colorbar shows normalized magnitude in dBFS.

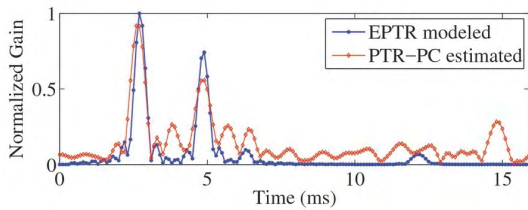


FIGURE 10. A CIR snapshot comparison. Envelope of complex baseband equivalent CIR obtained by PC estimation with PC-PTR (magenta) and by environmental focalization with EPTR (blue), for hydrophone 6 on May 27, slot number 4.

parameters can be seen as a by product of the EPTR communication system. The term “geometric parameters” denotes the physical parameters directly related to the source and receiver positions, *i.e.*, source-array range, source depth and the receiving array depth (using the shallowest hydrophone as reference).

Fig. 11 shows for snapshots 1 to 20 the evolution of the combination of geometrical physical parameters that generated the three best CIR replicas for the data collected on May 24 (a) and on May 27 (b): the best fitness maximum “a posteriori” parameter estimates (dash blue-circle), the second best fitness parameters (dash red cross) and the third best fitness data (dash green cross). It can be seen that there is a reasonably good trend between the three candidates for each geometric parameter, even though the data of May 27, shows a higher variation than that of May 24.

In addition to the parameters shown in Fig. 11, the geoacoustic parameters of the sediment layer shown in Table 1, are also used in the focalization process (not shown). For the scope of this work, their inclusion in the search space aims at improving the adjustment between replicas and observation

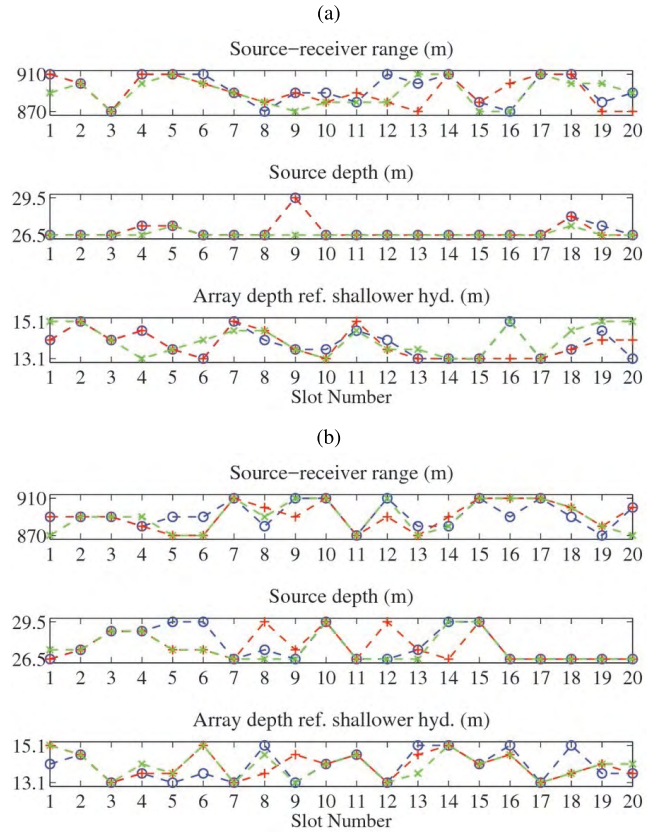


FIGURE 11. Maximum a posteriori geometric parameters obtained through environmental focalization for each slot of the data frame received on May 24 (a) and on May 27 (b). The three best fitness set of parameters are shown: maximum “a posteriori” set (blue circles), second maximum set (red cross) and third maximum set (green cross).

during the objective function optimization [21], [25]. Further, since there are physical parameters not inverted for, *i.e.*, parameters with fixed values along the optimization, it is expected to observe variability on the output inverted parameters that is not only due to their actual physical variability, but also due to the their ability to compensate those fixed parameters not considered for optimization. This procedure that divides the channel parameters in two component groups, one fixed and the other variable, is usual in matched-field inversion.

The compressional sound speed in the sediment repeatedly reaches the lower boundary of the search space along the time slots (not shown). At first, one is tempted to decrease the lower boundary of the search space, but since its value is 1480 m/s, already lower than the mean water sound speed, it was decided to maintain the search interval in order to avoid generating an excessively non-realistic environment, which scope would be to, probably, compensate other parameters not included in the search. This is the process known as acoustically-equivalent environment [26] or equivalent model [27] that we use here at our advantage for CIR replica channel equalization.

In this work the bottom half-space parameters were not optimized for because it is expected that at this

TABLE 3. Performance analysis of PC-PTR and EPTR.

May 24	PC-PTR	EPTR	Gain (dB)
MSE (dB)	-11.60	-12.53	0.93
BER	1.20×10^{-3}	3.64×10^{-4}	5.19
# errors (out of 71504)	86	26	
May 27			
MSE (dB)	-7.13	-10.80	3.67
BER	3.97×10^{-2}	2.92×10^{-3}	11.34
# errors (out of 71504)	2842	209	

high-frequency regime (carrier frequency at 26.5 kHz) the propagating signals have very small interaction with that region, due to strong attenuation on the seabed and rays refraction occurring only in the sediment layer.

More controversial is that, also the SSP was not optimized for during the focalization process. Instead, the profiles taken nearby to the STU receiving array of Fig. 4 were used. However, the SSP is an important modeling parameter since it directly influences the refraction of the propagating rays in the water column and its time variability has a certain impact on the CIR. The reason for not including the SSP in the search space was twofold: one is that there was no sufficient terrain information and two it would substantially increase the search space. The SSP difference between the two days makes May 24 data set a much benign channel that that of May 27, with a low distortion and a diagram constellation with low cluster variance and better performance, as shown in the metrics of table 3. The SSP of May 27 is significantly different from that of May 24, and shows a higher variability with, in general, worse results for both the PC-PTR and EPTR processors, although in both cases the EPTR yielded a visible gain over the conventional PC-PTR, actually with a higher gain in the “worst” day of May 27, as shown in Table 3.

3) COMMUNICATION PERFORMANCE ANALYSIS

The last point is to evaluate the performance of the communication system in recovering the transmitted message. This may be done in a variety of forms, one of which is by observing the received signal constellation diagram, as shown in Fig. 12 for May 24 with PC-PTR (a) and EPTR (b) and for May 27 with PC-PTR (c) and EPTR (d). It can be observed that the EPTR constellations are better separated than the PC-PTR constellations. This assertion is striking for the data set of May 27, plots (c) and (d). This reduced cluster variance means a clear soft-decision improvement.

Another, possibly more objective, form for performance evaluation is through bit error rate (BER) and mean square error (MSE). Table 3 shows the values of MSE, BER and number of wrong symbols of these constellations over the whole data horizon, where it is observed that the EPTR yields a considerable gain both on May 24 and on May 27. Observing the constellations and the numerical metrics it is clear that the performance of the system has been improved by using the EPTR processor.

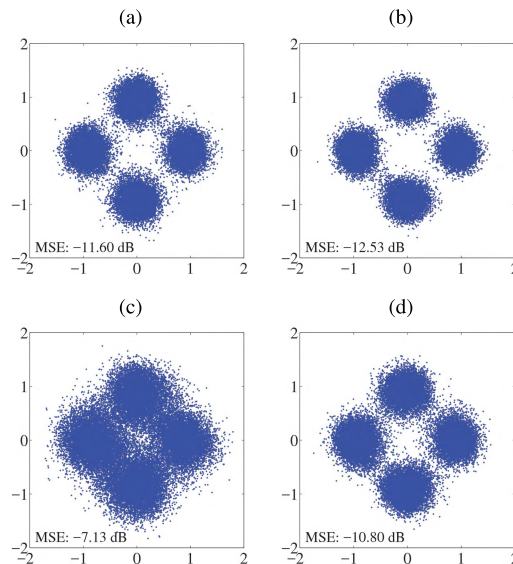


FIGURE 12. Constellation of the signal received on May 24, after being processed with PC-PTR (a) and EPTR (b), and for the signal received on May 27, after being processed with PC-PTR (c) and EPTR (d).

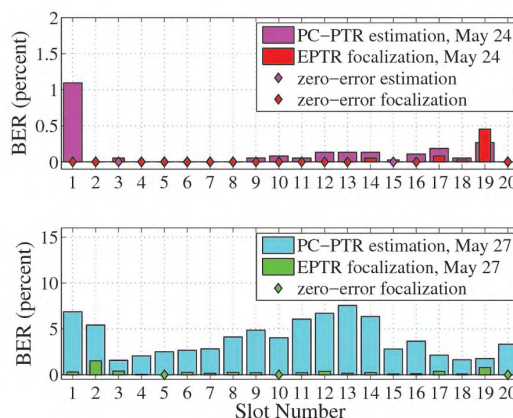


FIGURE 13. BER results per slot: May 24 data set (upper subplot), PC-PTR (magenta) and EPTR (red); May 27 data set (lower subplot), PC-PTR (cyan) and EPTR (green). The diamond marker denotes an error-free slot.

Fig. 13 shows, for each slot along the signal frame, the BER results of the signal collected on May 24 after being processed by PC-PTR (magenta) and by EPTR (red), and on May 27 after being processed by PC-PTR (cyan) and by EPTR (green). Observe that several slots of the May 24 data are error-free, both for the PC-PTR and the EPTR, while the EPTR results overcome the PC-PTR results in general, except for the slot number 19. On May 27, only the EPTR yields error-free slots and its performance by far overcomes the results reached with the PC-PTR.

Fig. 14 shows the soft-decision MSE results along the 20 slots of the signal frame, for May 24 data with PC-PTR processing (magenta circles/dashed line) and with EPTR (red circles/dashed line), and for May 27 with PC-PTR (cyan crosses/full line) and by EPTR (green crosses/full line). The EPTR results have a lower MSE than the PC-PTR both

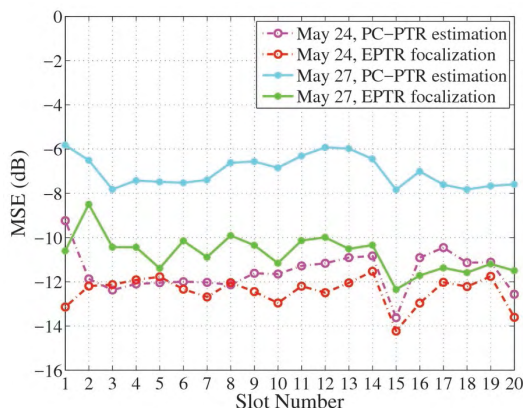


FIGURE 14. Mean square error of the received equalized communications signal for the full array. Results along the 20 slots in the signal frame with PC-PTR on May 24 (magenta), EPTR on May 24 (red), PC-PTR on May 24 (blue) and EPTR on May 27 (green).

on May 24 and on May 27. In particular, on May 27, EPTR outperforms PC-PTR by approximately 4 dB, which is the highest value over the whole data set processed in this work. Moreover, results shows a consistent improvement along the 20 seconds data frame.

IV. CONCLUSION

This paper presents results of coherent underwater acoustic communications that employ an environmental focalization algorithm for improving passive time-reversal performance. Environmental focalization works as a sub-processor that uses any available a priori or historical environmental information to search for numerical model outputs that best approach channel probe pulse compressed estimates. The fact that these model outputs are noise free while the originally used pulse compressed estimates are noisy, provide the potential for the processing gain.

The proposed EPTR algorithm is applied to real data sets acquired in two different days during the UAN'11 experiment carried out in Trondheim (Norway), over a range dependent shallow water 900 m long transect. QPSK modulated data packets were transmitted with a cNode-Mini Kongsberg modem at 4k bits/s during 20 s each day, in different environmental conditions and were received on a 16 channel vertical array. The results obtained show that EPTR outperforms standard PC-PTR by an amount varying from 1 to 4 dB, in MSE gain, over the two processed data records. The proposed method is shown to be robust yielding results that are nearly always equal or better than those provided by standard passive time-reversal, despite the considerable variation of channel responses both at micro-scale from second to second or from one day to the other. The results also show that the modeling errors (inevitably) present at the focalization algorithm output were small enough to still provide processing gain of the noise present in the pulse-compressed channel estimate. To some extent this method trades modeling errors for noise, with a net gain for the former.

The focalization algorithm provides enough detail to capture and to follow over time the essence of channel variability.

It is unknown whether that variability is due to sensor motion, surface agitation, currents or micro temperature changes, but a minimal set of physical parameters were able to track it and successfully undo channel paths by matched filtering the array receivers. The search space for the focalization was sufficiently small to be exhaustively covered, while still running in a reasonable time on a laptop computer.

To the authors best knowledge this is the first time that numerical modeling channel estimates were directly used for channel equalization of underwater acoustic communications with real data at an useful frequency range, say, over 20 kHz. In that regard, these results represent a step towards using the potential of connecting environment and channel compensation in field experiments.

ACKNOWLEDGMENT

The authors would like to thank the support of IEAPM-MB and LARSys.

REFERENCES

- [1] M. Stojanovic, "Underwater acoustic communications," in *Encyclopedia of Electrical and Electronics Engineering*, vol. 22, J. G. Webster, Ed. New York, NY, USA: Wiley, 1999, pp. 688–698.
- [2] J. G. Proakis, *Digital Communications*. New York, NY, USA: McGraw-Hill, 2008.
- [3] T. C. Yang, "Environmental effects on phase coherent underwater acoustic communications: A perspective from several experimental measurements," in *High Frequency Ocean Acoustics*, M. S. M. Porter and W. Kuperman, Eds. College Park, MD, USA: American Institute of Physics, 2004.
- [4] M. Stojanovic, J. Catipovic, and J. G. Proakis, "Adaptive multichannel combining and equalization for underwater acoustic communications," *J. Acoust. Soc. Amer.*, vol. 94, pp. 1621–1631, Sep. 1993.
- [5] A. Song, M. Badiy, and V. McDonald, "Multichannel combining and equalization for underwater acoustic MIMO channels," in *Proc. IEEE/MTS Oceans*, Sep. 2008, pp. 1–6.
- [6] D. Jackson and D. Dowling, "Phase conjugation in underwater acoustics," *J. Acoust. Soc. Amer.*, vol. 89, pp. 171–181, Apr. 1991.
- [7] D. Rousset, J. Flynn, J. Ritcey, and W. Fox, "Acoustic communication using time-reversal signal processing: Spatial and frequency diversity," in *High Frequency Ocean Acoustics*, M. Porter, M. Siderius, and W. Kuperman, Eds. College Park, MD, USA: American Institute of Physics, 2004.
- [8] J. Gomes, A. Silva, and S. Jesus, "Adaptive spatial combining for passive time-reversed communications," *J. Acoust. Soc. Amer.*, vol. 124, pp. 1038–1053, Aug. 2008.
- [9] H. Song, "Time reversal communications with a mobile source," *J. Acoust. Soc. Amer.*, vol. 4, pp. 2623–2626, Oct. 2013.
- [10] G. Zhang, "Coherent underwater communication using passive time reversal over multipath channels," *J. Elsevier Phys. Commun.*, vol. 72, pp. 412–419, Apr. 2011.
- [11] M. Stojanovic, "Retrofocusing techniques for high rate acoustic communications," *J. Acoust. Soc. Amer.*, vol. 117, no. 3, pp. 1183–1185, 2005.
- [12] H. C. Song, W. S. Hodgkiss, W. A. Kuperman, M. Stevenson, and T. Akal, "Improvement of time-reversal communications using adaptive channel equalizers," *IEEE J. Ocean. Eng.*, vol. 31, no. 2, pp. 487–496, Feb. 2006.
- [13] H. C. Song, P. Roux, W. S. Hodgkiss, W. A. Kuperman, T. Akal, and M. Stevenson, "Multiple-input-multiple-output coherent time reversal communications in a shallow-water acoustic channel," *IEEE J. Ocean. Eng.*, vol. 31, no. 1, pp. 170–178, Jan. 2006.
- [14] M. J. Hinich, "Maximum-likelihood signal processing for a vertical array," *J. Acoust. Soc. Amer.*, vol. 54, pp. 499–503, Sep. 1973.
- [15] C. S. Clay, "Optimum time domain signal transmission and source location in a waveguide," *J. Acous. Soc. Amer.*, vol. 81, p. 660, Sep. 1987.
- [16] A. Tolstoy, *Matched Field Processing for Underwater Acoustics*. Singapore: World Scientific, 1993.

- [17] A. B. Baggeroer, W. A. Kuperman, and P. N. Mikhalevsky, "An overview of matched field methods in ocean acoustics," *IEEE J. Ocean. Eng.*, vol. 18, no. 4, pp. 401–424, Oct. 1993.
- [18] W. Munk and C. Wunsch, "Ocean acoustic tomography: A scheme for large scale monitoring," *Deep Sea Res.*, vol. 26, pp. 123–161, Sep. 1979.
- [19] W. Munk, P. Worcester, and C. Wunsch, *Ocean Acoustic Tomography*. Cambridge, U.K.: Cambridge Monographs on Mechanics, 1995.
- [20] Z. H. Michalopoulou, "Robust multi-tonal matched-field inversion: A coherent approach," *J. Acoust. Soc. Amer.*, vol. 104, pp. 160–170, Sep. 1998.
- [21] M. D. Collins and W. A. Kuperman, "Focalization: Environmental focusing and source localization," *J. Acoust. Soc. Amer.*, vol. 90, pp. 1410–1422, Sep. 1991.
- [22] M. B. Porter, *The BELLHOP Manual and Users Guide*, Heat, Light, Sound Res., La Jolla, CA, USA, Jan. 2011.
- [23] A. Caiti et al., "Linking acoustic communications and network performance: Integration and experimentation of an underwater acoustic network," *IEEE J. Ocean. Eng.*, vol. 38, no. 8, pp. 758–771, Oct. 2013.
- [24] T. Husoy, M. Pettersen, B. Nilsson, T. Öberg, N. Warakagoda, and A. AbdiLie, "Implementation of an underwater acoustic modem with network capability," in *Proc. IEEE Oceans Conf.*, Apr. 2011, pp. 1–10.
- [25] C. Soares, S. M. Jesus, and E. Coelho, "Environmental inversion using high-resolution matched-field processing," *J. Acoust. Soc. Amer.*, vol. 122, no. 6, pp. 3391–3404, 2007.
- [26] S. E. Dosso and P. Zakarauskas, "Matched-field inversion for source location and equivalent bathymetry," in *Full Field Inversion Methods in Ocean and Seismo-Acoustics (Modern Approaches in Geophysics)*, vol. 12, H. Diachok, O. Caiti, A. Gerstoft, and P. Schmidt, Eds. Amsterdam, The Netherlands: Springer, 1995.
- [27] N. E. Martins, "Acoustic-oceanographic data fusion for prediction of oceanic acoustic fields," Ph.D. dissertation, Faculty Sci. Technol., Univ. Algarve, Faro, Portugal, 2014.



sparse channel equalization, and also acoustic inversion and ocean acoustics.

LUSSAC P. MAIA received the M.Sc. degree in ocean engineering, geoacoustic inversion branch, Federal University of Rio de Janeiro, Brazil, in 2010. He is currently pursuing the Ph.D. degree in electronics and telecommunications engineering, signal processing branch, with the University of Algarve, Portugal. From 2011 to 2013, he was the Head of the Acoustic Measurement Department, CASOP, Brazilian Navy. His research interests include underwater acoustic communications,



environmental-based equalization, and ocean acoustic propagation modeling and signal processing for high-rate underwater communications.

ANTÔNIO SILVA received the M.Sc. degree from the University of Algarve, Faro, Portugal, in 1998, and the Ph.D. degree in electrical and computer engineering from the Instituto Superior Técnico, Lisbon, Portugal, in 2009. He is currently an Adjunct Professor, and the Director of the M.Sc. course in electrical engineering and electronics from the Instituto Superior de Engenharia, University of Algarve. His research interests include underwater acoustic communications,



environmental-based equalization, and ocean acoustic propagation modeling and signal processing for high-rate underwater communications.

SÉRGIO M. JESUS received the D.Sc. degree in engineering sciences from the University of Nice, France, in 1986. From 1985 to 1992, he was a Staff Scientist with the SACLANT Undersea Research Centre, Ambient Noise and Signal Processing Groups, La Spezia, Italy. He was involved in underwater acoustic field noise directionality and early studies on target detection using matched field processing. In 1992, he joined the Electronics and Computation Department, University of Algarve, Faro, Portugal, where he is currently a Full Professor. His research interests include underwater acoustics signal processing, model-based inversion, and also ocean and seafloor tomography and their applications. Dr. Jesus is a member of the IEEE Signal Processing Society, the EURASIP, and the Acoustical Society of America.

...